Nonlinear Landau damping of plasma waves with orbital angular momentum

D. R. Blackman [1,2], R. Nuter [2], Ph. Korneev [3,4] and V. T. Tikhonchuk [2,5]

[1] *Mechanical and Aerospace Engineering, University of California San Diego, 9500 Gilman Drive, La Jolla, California 92093-0411, USA*

[2] *CELIA, University of Bordeaux, CNRS, CEA, 33405 Talence, France*

[3] *National Research Nuclear University "MEPhI" (Moscow Engineering Physics Institute), Moscow, 115409 Russia*

[4] *P. N. Lebedev Physics Institute, Russian Academy of Sciences, 119991 Moscow, Russia*

[5] *ELI-Beamlines, Institute of Physics, Czech Academy of Sciences, 25241 Dolní Břežany, Czech Republic*

(Received 30 April 2020; accepted 23 July 2020; published 23 September 2020)

We present, using three-dimensional particle-in-cell simulations, an observation that orbital angular momentum (OAM) is transferred to resonant electrons proportionally to longitudinal momentum when Laguerre-Gaussian plasma waves are subjected to Landau damping. A higher azimuthal mode number leads to a larger net orbital angular momentum transfer to particles traveling close to the phase velocity of the plasma wave, implying a population of electrons that are orbiting the same center of rotation as the plasma wave. This observation has implications on magnetic field excitation as a result of the formation and damping of OAM plasma waves. The energy distributions of electrons in damping Laguerre-Gaussian plasma waves are significantly changed as a function of azimuthal mode number. This leads to larger numbers of lower energy particles tending towards a significant narrowing of the energy distribution of accelerated particles.

DOI: 10.1103/PhysRevE.102.033208

I. INTRODUCTION

Electromagnetic waves carrying orbital angular momentum (OAM), described as Laguerre-Gaussian solutions to the paraxial equation in cylindrical geometry [1], have a variety of applications in optics. Applications with low-intensity beams include those for compact storing of information, nanoscale imaging, and manipulation [2]. More recently applications at higher intensities are showing the potential of OAM light in particle focusing and acceleration, generation of strong plasma waves, and quasistatic magnetic fields [3–6].

A proper description of the propagation of electromagnetic waves with OAM through a plasma requires the understanding of excitation and evolution of electrostatic waves (plasmons) carrying OAM [7]. In addition to this, these OAM plasmons may have applications of their own, as several studies [8,9] show, for the generation of complex quasistatic magnetic fields.

The description of OAM plasmons damping requires the kinetic framework. However, the Laguerre-Gaussian (LG) functions are not the eigenfunctions of the electron kinetic equation. For this reason, a simplified consideration [10] leads to an inaccurate expression of the dispersion, and thus of the phase velocity, and damping of these waves even in the linear regime. A more consistent approach using the expansion on the paraxial parameter—the ratio of the plasma wavelength $2\pi/k$ to the radial width of the wave packet w_b (or more conveniently written as $1/kw_b$)—leads to dispersion and damping coefficients being shown to be strongly mode dependent in certain regimes [8].

For an electron, with a sufficiently small initial velocity v, traveling through a low-amplitude plasma wave, the electric field of an OAM plasma wave reversibly transfers linear momentum and orbital momentum to the particle during one half cycle and then back in the second one. When the plasma wave is damped, this symmetry is broken and momentum, both linear, and possibly orbital angular momentum, can be transferred. Calculations have been performed to find the proportion of angular momentum transferred from the electrostatic wave to individual particles [11]. In this paper we study the irreversible transfer occurring via Landau damping in the nonlinear regime where particle trapping can occur.

II. LINEAR THEORY

A. OAM plasma waves

To aid in understanding of this study we briefly restate the formalism used for description of OAM plasma waves [8]. A small-amplitude plasma wave is described by an electrostatic potential Φ and electron distribution function f related by the Poisson equation, SI units are used throughout this paper with noted exceptions:

$$\nabla\Phi = \frac{e}{\epsilon_0}\delta n_e = \frac{e}{\epsilon_0}\int d\mathbf{v}\delta f_e, \tag{1}$$

where e is the unitary charge, ϵ_0 is the vacuum permittivity, δf_e the perturbed distribution function, and δn_e the charge density. The solutions to the paraxial equation in the limit $1/kw_{b,0} \ll 1$ are of the form, with k being the wave number and ω the frequency of the plasma wave:

$$\Phi(z, r, \theta, t) = \sum_{p,l} \phi_{p,l} F_{p,l} \exp(-i\omega t + ikz + il\theta + i\psi_{p,l} + iqX), \tag{2}$$

 ©2020 American Physical Society

$$f(z, r, \theta, \mathbf{v}, t) = \sum_{p,l} f_{p,l}(\mathbf{v}) F_{p,l} \exp(-i\omega t + ikz + il\theta + i\psi_{p,l} + iqX). \quad (3)$$

Here q is the term accounting for front curvature, $X = r^2/w_b^2$ is the normalized radial coordinate, and $\psi_{p,l}$ is the Gouy phase. For this study we consider a plasma wave with the constant beam waist w_b. This means considering the structure within the Rayleigh zone $|z| \ll z_R$, such that the contributions of q and $\psi_{p,l}$ are ignored. $F_{p,l}$ is the Laguerre-Gaussian function given by

$$F_{p,l}(X) = C_{p,l} X^{|l|/2} L_p^{|l|}(X) e^{-X/2}, \quad (4)$$

$L_p^{|l|}$ is a generalized, or associated, Laguerre polynomial with radial mode integer $p \geqslant 0$ and azimuthal mode integer l, and $C_{p,l} = \sqrt{p!/(|l|+p)!}$ is a normalization factor to ensure that solutions are orthonormal. As presented in Ref. [8] for the Vlasov equation, the solutions given in Eqs. (2) and (3) are not plasma wave eigenmodes, and so neighboring modes are coupled in higher orders of the paraxial parameter $1/kw_b$.

The dielectric permittivity for a plasma supporting a wave with OAM, in the case $|z| < z_R$, reads

$$\epsilon(\omega, k) = 1 + \frac{e^2}{\epsilon_0 k^2} \int d\mathbf{v} \left[-1 + \frac{\omega(\omega - kv_z)}{(\omega - kv_z)^2 - (2p + |l| + 1)v_\perp^2/2w_{b,0}^2} \right] \partial_\varepsilon f_{e0} = 0, \quad (5)$$

where $v_\perp$ and v_z are the perpendicular and axial velocity components, f_{e0} is the unperturbed distribution function. For this analysis the distribution f_{e0} is considered to be a Maxwell distribution. The solution of this equation in the limit $\omega \gg kv_{\rm th}$, where $v_{\rm th} = \sqrt{T_e/m_e}$ is the electron thermal velocity, T_e the electron temperature in energetic units, and m_e is the electron mass, can be found by using a standard expansion procedure. The real part of Eq. (5) gives the plasma wave dispersion:

$$\omega^2 \approx \omega_{\rm pe}^2 \left(1 + 3k^2\lambda_{\rm De}^2 + \frac{2p + |l| + 1}{k^2 w_{b,0}^2} \right), \quad (6)$$

where $\omega_{\rm pe} = \sqrt{e^2 n_{e0}/m_e\epsilon_0}$ is the plasma frequency and $\lambda_{\rm De} = v_{\rm th}/\omega_{\rm pe}$ is the electron Debye length, e the electron unitary charge, and m_e the electron mass. The last term in this dispersion relation accounts for the OAM and finite beam waist and makes a nonthermal contribution to the frequency. To find the damping rate the residues in the resonance terms on the right-hand side of Eq. (5) are taken. The Landau resonance in the case for OAM plasma waves is split into two resonances $v_z^\pm = \omega/k \pm (v_\perp/kw_{b,0})\sqrt{p + (|l|+1)/2}$, which are shifted with respect to the standard linear resonance $v_z = \omega/k$ for a plane wave. The calculation of the corresponding integrals of these residues leads to the damping rate [8,11]:

$$\frac{\gamma_L}{\omega} \approx \sqrt{\frac{\pi}{8}} \frac{1}{k^3\lambda_{\rm De}^3} \exp\left(-\frac{\omega^2}{2k^2 v_{\rm th}^2} \right) R\left[\frac{\sqrt{p + (|l|+1)/2}}{k^2\lambda_{\rm De} w_{b,0}} \right]. \quad (7)$$

Here $\gamma_L = -\mathrm{Im}\,\omega$, the function $R(\xi)$ accounts for the OAM and can be written as

$$R(\xi) \equiv 1 + \sqrt{\frac{\pi}{2}}\xi \exp\left(\frac{\xi^2}{2}\right) \mathrm{erf}\left(\frac{\xi}{\sqrt{2}}\right) \quad (8)$$

where "erf" denotes the error function and $\xi = \sqrt{p + (|l|+1)/2}/k^2\lambda_{\rm De} w_{b,0}$. In the limit where $\xi \to 0$, the plasma wave damping rate is reduced to the Landau damping of a plane wave. For a plasma wave with OAM, or finite beam waist, the contributions due to $\xi \neq 0$ are of the same order for the dispersion and for the damping. The OAM carried by plasma waves results in the increase the dispersion and damping for long wavelengths under the conditions where $(k\lambda_{\rm De})^2 \lesssim \lambda_{\rm De}/w_{b,0}$.

B. Electric field

For simplicity we consider here a structure of a single mode p and use the electric potential given in Ref. [8] containing only one term characterized by the amplitude $\phi_{p,l}$:

$$\Phi(z, r, \theta) = \phi_{p,l} F_{p,l}(X) \cos(kz - \omega t + l\theta). \quad (9)$$

The electric field is found by taking the gradient of the potential:

$$E_z = E_0 F_{p,l}(X) \sin(kz - \omega t + l\theta), \quad (10)$$

$$E_\theta = \frac{lE_0}{kw_b} X^{-1/2} F_{p,l}(X) \sin(kz - \omega t + l\theta), \quad (11)$$

$$E_r = -2\frac{E_0}{kw_b} X^{1/2} F'_{p,l}(X) \cos(kz - \omega t + l\theta), \quad (12)$$

where $E_0 = k\phi_{p,l}$ is the amplitude of the axial electric field. The axial field dominates, and the transverse field amplitudes are smaller by a factor $1/kw_b$. When looking at Eqs. (11) and (12), one can immediately observe from these two equations that $E_\theta/E_z = l/kr$.

A previously published calculation [11] has been performed to find the momentum gain from the electron equation of motion in an electric field described by Eqs. (10), (11), and (12). This calculation is made assuming a small first-order change, which would still be in the realm of a small deviation occurring per plasma oscillation. This calculations yields a ratio of $\Delta v_\theta/\Delta v_z = l/kr$ or considering the change in radial position as well $\Delta(rv_\theta)/\Delta v_z = l/k$. This relation can be written in terms of the orbital angular momentum as $\Delta l_z/\Delta p_z = l/k$ where Δl_z is the change in the z component of the particle orbital momentum.

III. NUMERICAL SIMULATION SETUP

A. Plasma wave amplification

For this study the particle-in-cell (PIC) code OCEAN [12] is used. To create a stable plasma wave a similar initialization to that described in Refs. [8,11] can be used to adiabatically drive a plasma wave for a small number of oscillations, a description of the amplification process is presented in the Appendix. An electric field is volumetrically imposed according to Eqs. (10), (11), and (12). Several simulations are run, each for a single mode, the first with a standard Gaussian profile, with $p = 0$ and $l = 0$, the remaining three simulations with $p = 0$ and $l = 1$, 2, and 4. The simulation box boundaries are reflecting on the transverse edges, to preserve any OAM particles may have gained, and periodic along the wave propagation axis in order that the wave can be excited.

For these simulations a plasma is set up so that a cold phase velocity of $\omega_{\rm pe}/k = 0.53\,c$ is chosen, with an initial temperature $T_e = 0.03\,m_e c^2 \simeq 15$ keV such that $v_{\rm th} = 0.173\,c$. The resolution is set so that $\Delta x = 0.8278\,\lambda_{\rm De}$ and $\Delta t = 0.01318\,T_{\rm pe}$, where $T_{\rm pe} = 2\pi/\omega_{\rm pe}$ is the plasma wave period. The grid resolution is observed to be sufficient to ensure energy conservation and other nonphysical effects for at least $4000\,\Delta t$. The plasma wave transverse width is $w_b = 0.95\,\lambda_{\rm pe}$, where $\lambda_{\rm pe} = 2\pi/k$ is the plasma wavelength, so that the paraxial parameter is $kw_b = 6$.

The waves are initially driven with the described electric field over five periods with a dimensionless amplitude $eE_0/m_e\omega_{\rm pe}c = 0.08$. The amplitude of the plasma waves reach only $eE_0/m_e\omega_{\rm pe}c \sim 0.025$, due to a slight mismatching between the phase of the imposed electric field and the plasma response, and due to the damping of the wave occurring during the amplification process. The amplitudes of the different modes compare well between simulations; the total energy of the plasma wave in each run varies less than 3% from the mean plasma-wave energy across all simulations.

The simulation parameters are chosen foremost with the aim of studying the wave-particle interaction in three dimensions and at the same time being achievable computationally, while also not having a Landau damping rate so high that no plasma wave survives. With the second concern being having some Landau damping at velocities that are observable within the PIC code given the limited number of particles per cell achievable in three dimensions. The amplitude of the wave is also carefully chosen so that the resulting plasma wave is not close to the wave-breaking regime, while still being visible above PIC noise.

B. Model for the tail of electron distribution function

When generating a distribution of electrons in a 3D PIC simulation a good resolution of higher energy regions of the distribution function, e.g., regions very far from the mean velocity, is necessary in our case. To achieve a reasonable resolution for the diagnostics related to the distribution function, for a moderate temperature plasma ($v_{\rm th} \ll c$), the velocity distribution function along the wave propagation axis is split into three parts. The first part being a truncated Gaussian distribution such that the distribution is cut of at $v_z < |v_s|$ and is symmetrical about the mean velocity. The remaining two parts consist of tail distributions truncated such that $|v_z| > v_s$. For the main body distribution a Box-Mueller transform [13] can be used to generate a Maxwellian distribution followed by a simple accept-reject method to make the cutoffs at the $\pm v_s$ edges of the distribution. For the last two parts the method described in chap. 9 in Devroye [14], for sampling a Gaussian tail distribution is efficient enough that it can be employed to generate the two tail distributions for a split value of $v_s = 2.5\,v_{\rm th}$. The result is two electron species; the first consisting of macroparticles with larger statistical weights to represent the bulk of the electrons with lower energies, the second a species with smaller statistical weights accounting for higher energy particles.

When tested using a plasma wave with $v_{\rm ph} = c$, so that no damping will occur (as in Ref. [8]), the simulations with multiple electron species and single species produce identical results. However, the simulations with lower values of $v_{\rm ph} \simeq 3\,v_{\rm th}$, where Landau damping is expected to be stronger, with just a single species of electrons were seen to artificially suppress Landau damping as there are not enough macroparticles in the correct region to exchange energy with the plasma wave. When testing the number of particles required in the extra species of electrons to initiate damping, a small number were added to each simulation run until the behavior was seen not to change significantly from run to run. The electrons in each simulation are split into two species, with 100 particles per cell for the main-body distribution, and 20 particles per cell for both tail ($|v_z| > v_s$) distributions.

For this study only a split along the wave propagation direction is considered. While it is possible to add extra particles in the transverse direction it is not necessary for observing Landau damping of a wave with a phase velocity $v_{\rm ph} \gg v_{\rm th}$.

IV. SIMULATION RESULTS

A. Nonlinear Landau damping and particle trapping

Finding a regime where linear Landau damping is clearly observable in a 3D PIC environment, while still resolving relevant processes, is extremely challenging; for a full discussion see the Appendix. Linear Landau damping operates over a time shorter than the time required for particle trapping, and the characteristic time of wave evolution is a few damping times. Consequently, the linear regime is realized for $\sqrt{eE_0k/m_e} = \omega_b \ll \gamma_L$ (where ω_b is the bounce frequency), the nonlinear damping regime is realized in the opposite case. The linear damping condition poses a limit on the wave amplitude $E_0 \ll \gamma_L^2 m_e/ek$. Using the value for the Landau damping of a Gaussian wave, calculated in Table I, the amplitude of the wave is required to be $ekE_0/m_e\omega_{\rm pe}c \ll 0.005$ for the damping to be in the linear regime. Producing a low-amplitude wave that is still observable over numerical noise requires grid resolutions and particle numbers computationally prohibitive in a 3D regime. However, obtaining results for a relatively stable nonlinear regime is achievable.

The conditions in the presented PIC simulations, along with the extra resolution provided by the additional particle species, give rise to nonlinear Landau damping as the bounce

TABLE I. Values predicted using linear theory for the phase velocity and damping rate, the value of $k\lambda_{De} = 0.3264$. The first row shows the predicted dispersion ω/ω_{pe}, the second row shows the predicted phase velocity $\omega/kc = v_{ph}$ (c), the third row shows the minimum momentum p_{ph} that an electron can have traveling at the phase velocity. The fourth and fifth rows show details of the calculation of the linear regime Landau damping rate; the fourth row shows the value ξ used in Eq. (8), the fifth row shows the result of Eq. (8), and the sixth row shows the predicted Landau damping rate, γ_L/ω, calculated using Eq. (7). The damping rate for the Gaussian wave is calculated using a value of $\xi = 0$ for reference. It is worth noting that the predicted damping rates of the modes with $l > 1$ are slightly reduced as the increase in the phase velocity outweighs the contribution of the OAM.

l	plane wave	1	2	4
ω/ω_{pe}	1.160	1.173	1.184	1.208
ω/kc	0.615	0.621	0.628	0.640
p_{ph}	0.780	0.792	0.807	0.833
ξ	–	0.511	0.625	0.807
$R(\xi)$	–	1.285	1.446	1.814
γ_L/ω	0.0325	0.0369	0.0359	0.0349

frequency $\omega_b = \sqrt{eE_0k/m_e} \simeq 0.7\omega_{pe}$ is only slightly smaller than the plasma frequency. The maximum amplitude achieved in the simulations is lower than the wave-breaking threshold [15] (i.e., $eE_0/m_e\omega_{pe} < v_{ph}$), and so wave breaking is not observed. Another nonlinearity to note is that the phase velocity (at the lowest condition for a Gaussian mode $\omega/k = 0.61\ c$ from the Bohm-Gross dispersion), while not strongly relativistic (an electron with a velocity of only the phase velocity will have relativistic factor $\gamma = 1.26$) will lead to particles accelerating into relativistic regimes.

While these conditions present more difficulty in analysis and linking to linear theory, they do provide an interesting test to observe the transfer of OAM from an electrostatic plasma wave to resonant particles. The rotation in phase space (v_z, z) for nonlinear Landau damping is observable in Fig. 1, in the Gaussian case as we can integrate over the whole transverse plane. In the case of higher LG modes this rotation is seen when changing variables to "untwisted" coordinates. The phase of a planar plasma wave $\phi_{l,pe} = kz - \omega t$, an electron traveling at a speed similar to ω/k sees an approximately stationary wave. In the case of the twisted wave there is an additional coordinate in the phase $\phi_{OAM,pe} = kz - \omega t + l\theta$ and for a copropagating electron the phase depends on the azimuthal angle as $z + l\theta/k$. Therefore, phase rotation is included in the "untwisted" phase so that the axial coordinate is chosen as $\tilde{z} = z + l\theta/k$. An important relation between the axial and azimuthal momenta can be obtained from the equation of electron motion in the plasma wave: $d\mathbf{p}/dt = e\nabla\Phi$. Indeed, by using Eq. (9) and assuming that the particle is not displaced radially we find in the nonrelativistic limit the following relation between p_z and p_θ:

$$krp_\theta - lp_z = Am_ec, \tag{13}$$

where A is a dimensionless constant with the expected value of 0. This means that average axial and orbial momentum are in a linear relationship. Evidently, this is valid only for particles

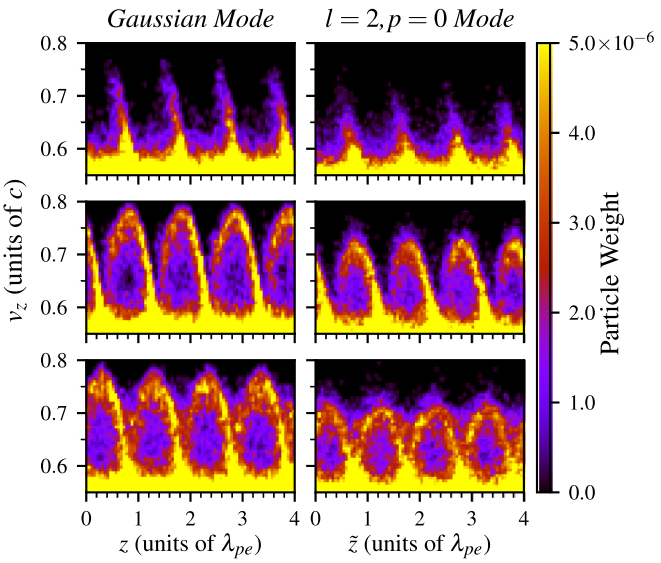

FIG. 1. Phase plots of v_z vs z at different times for the Gaussian beam (left) and an $l = 2$ Laguerre-Gauss beam, the top row shows the simulations at $t = 3.1\ T_{pe}$, the second row $t = 6.3\ T_{pe}$, and the last row at $t = 9.4\ T_{pe}$ after the simulation has started. These plots are calculated by integrating over the whole range of r and θ. The Gaussian wave clearly shows rotation in the v_z, z space; this is not visible for the Laguerre-Gauss wave until the appropriate variable $(v_z, \tilde{z})$ is selected, where $\tilde{z} = z + l\theta/k$. As there is only a single mode with a single phase velocity in each simulation rotation is visible only in the positive v_z direction.

close to the phase velocity v_{ph} of the plasma wave, as at lower v_z the potential averages to zero.

There are three distinct periods of time during the simulations, which need to be considered. The first period $t = 0 - 5\ T_{pe}$, is the time during which the plasma wave is amplified, with an increase in energy for both fields and particles. The second period $t = 3 - 4\ T_{pe}$ can be defined as a span of time, where a quasilinear Landau damping occurs (where $dE_0/dt < 0$, e.g., the amplitude decreases at a slower rate than linear theory predicts, but has not yet saturated; see Table I). Here the electric field energy decreases, while the particle energy rises at the same rate. The final period $t > 8 - 9\ T_{pe}$, being the span of time where there is a dynamic exchange between the electric field energy and particle energy. As the damping rate is dependent on the gradient of the distribution function around the phase velocity, it can be expected that the distribution function is flattened out around the phase velocity starting during the second period and completing in the third period; this can be seen in Fig. 2.

An additional indication of nonlinear behavior is the reduction of the resonant frequency, typical for nonlinear Landau damping interactions, where a plateau is created in the distribution function due to trapped particles [16–18]. Trapped particles are spatially bound and act in competition to the driving plasma wave, so reducing the restoring force, which consequentially reduces the frequency of the plasma wave. A discussion of the role of trapped particles in the alteration of the resonant frequency can be found in Ref. [19]. The phase velocity can be calculated by measuring the frequency of the

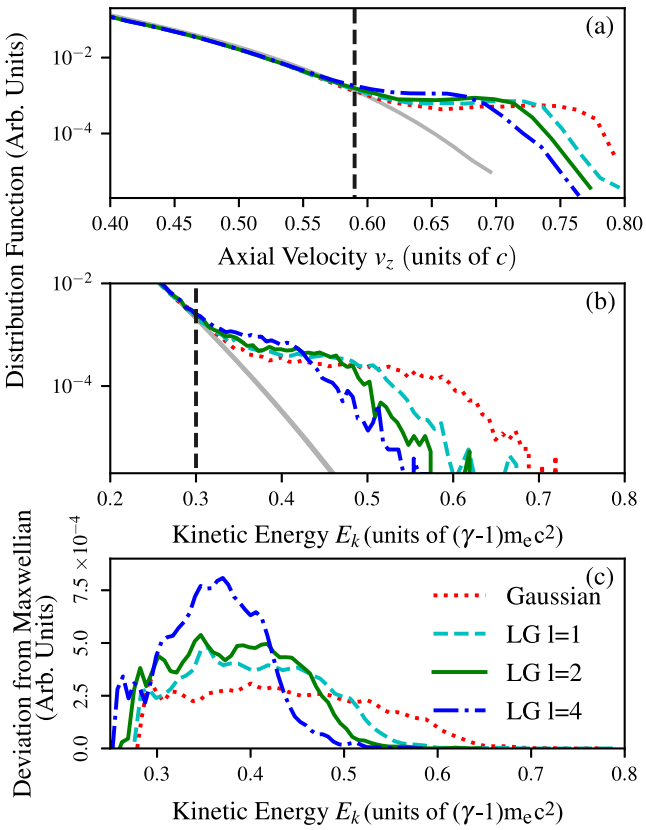

FIG. 2. Distribution of the particles on velocity in the axial direction (a), on energy (b), and deviation from the Maxwellian (c), at time $t = 5\ T_{\rm pe}$, or five plasma periods after amplification has finished. The solid light gray line shows the initial conditions for the simulations. The red dotted line shows the distribution for the Gaussian wave simulation, the cyan line for the case of LG mode $l = 1$, the green dashed line for $l = 2$, and the solid blue line for $l = 4$. The vertical dashed black line in plot (a) shows the magnitude of the measured phase velocity. The vertical dashed gray line in plot (b) shows $E_k = 0.30\ m_e c^2$ relevant to Fig. 3.

wave by taking the Fourier transform over the time domain in the electric field measured at several points in space. The points are located at the radial position of the peak in E_z for each mode, and at azimuthal angles $\theta = 0, \pi, \pi/2$, with z being equally spaced along the both length. The first 20 $T_{\rm pe}$ after the amplification period is chosen as the time domain so that there is enough accuracy to determine differences in the phase velocity. When taking the longitudinal electric field at these points E_z the measured value is $\omega/\omega_{\rm pe} = 1.12 \pm 0.01$ (or $v_{\rm ph} = 0.59\ c$ assuming constant k), which corresponds to a plasma frequency lower than the Bohm-Gross dispersion predicts. This value is also lower than the dispersion calculated according to Eq. (6) (see Table I), which can be related to the nonlinear frequency shift due to the trapped particles. There is no observable change in the phase velocity as a function of l in this regime, that is, the nonlinear frequency shift increases with orbital momentum.

The average transverse transit time of an electron moving across the plasma wave with a thermal velocity is approximately 6 $T_{\rm pe}$, while the approximate bounce period is ~1.4 $T_{\rm pe}$. This indicates, that while particles will remain trapped for some time, there is some irreversible transverse loss of energy from the wave to trapped particles.

There are two caveats to note, while analyzing the numerical results obtained in the setup described above. The first caveat is that the theory developed in previous works [8,11] supposes, for simplicity, a Maxwellian distribution, which, given the magnitude of the phase velocity $v_{\rm ph} \sim 0.6\ c$, may not be sufficient. Moreover, the Landau damping rate is a function of the derivative of the distribution function $df/{\rm d}v_z$ around the resonance region $v_z \sim v_{\rm ph}$, which is slightly shallower in the Maxwellian distribution when compared to the more realistic (for $T_e \to m_e c^2$) Maxwell-Jüttner distribution applying for relativistic electrons. The second caveat is that there are a finite number of particles in a periodic box. In this case the alteration of $df/dv_z|_{v_{\rm ph}}$ is much more significant as the gradient parallel to the wave propagation direction becomes flattened around phase velocity $v_{\rm ph}$, and so less momentum is transferred from the electrostatic wave to the particles. This may lead to a significant problem in comparing the measured phase velocity and damping rate that occurs in simulations like this to theoretical models, which assume fixed distribution functions. However, in the case of the nonlinear damping of a plasma wave, an appreciation of how momentum is transferred from the wave to the particles is possible and presented below.

B. Energy distribution

It is important to note that in each simulation the same amount of energy is input via the amplification process, the same temperature is initially selected, and that the distribution function for particles with energies less than ~0.30 $m_e c^2$ remain unchanged throughout the length of the simulation (more than 2000 time steps). Despite the fact that the low-energy particle behavior is similar in each simulation, the distribution of particles with energies higher than 0.30 $m_e c^2$ is quite different. The first difference is the shape of the distribution function [though the total energy is roughly constant; see Fig. 2(b)]. The second difference is in the distribution of energy among the three components of velocity v_z, v_θ, and v_r (see Fig. 3).

In each of the simulations the energy distribution derivative around the high-energy region [Fig. 2(b)] starts to decrease almost immediately as the plasma-wave is amplified. After approximately three to four periods after the amplification of the wave (approximately eight to nine plasma periods) a steady state is reached, where the energy transfer between the electric field and the particles becomes reversible and the rate of change of both becomes zero.

The distribution of particles in the high-energy tail is significantly different depending on the mode chosen [see Fig. 2(b)]. The Gaussian mode promoting particles to higher energies (with a maximum ~0.7 $m_e c^2$). The modes with larger l have larger numbers of particles accelerated but to lower energies (with a maximum of ~0.55 $m_e c^2$ in the case where $l = 4$). An interesting point to note is the reduction in the number of particles with very high energies at higher l. For $l = 4$ the distribution of energy of the accelerated particles is significantly narrower than those with lower mode numbers.

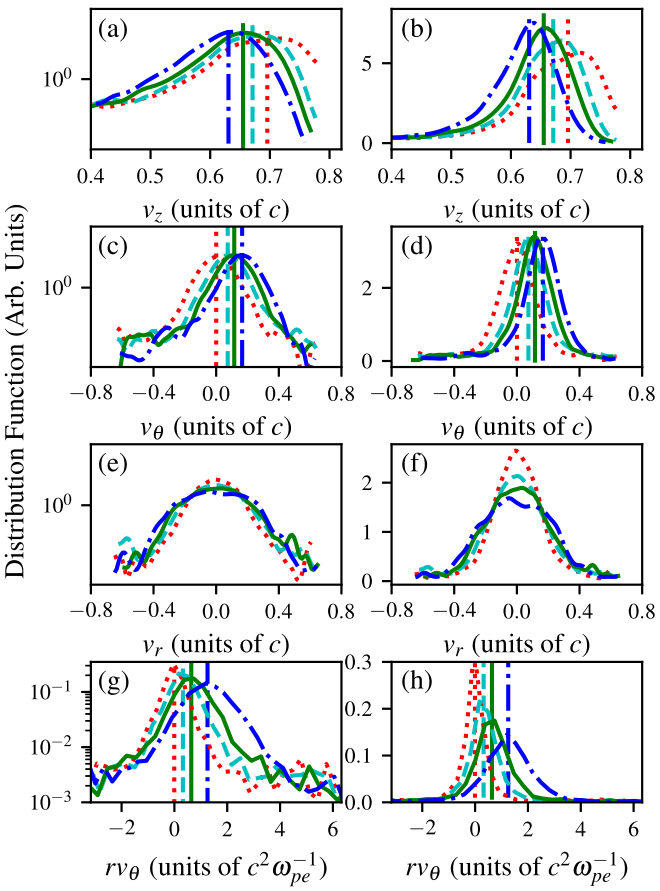

FIG. 3. Velocity distributions for particles with energies over $E_k > 0.3\, m_e c^2$, split into the axial z direction (a, b), azimuthal θ direction (c, d), radial r direction (e, f), and the distribution of rv_θ (g, h). The plots on the left have a logarithmic scaled y axis, while the plots on the right have a linear scale; the data are identical. Data taken at time $t = 5\ T_{\rm pe}$, or 5 plasma periods after amplification has finished. This plot uses the same line styles as in Fig. 2. The vertical lines show the average velocity for each component except the radial velocity plot where $\langle v_r \rangle = 0$ for all simulations. The lines shown here are smoothed using a moving average over five bins.

C. Momentum distribution

The largest differences in resonant electron behavior between the modes are apparent in the distribution of momentum when resolved into axial p_z, azimuthal p_θ, and radial p_r components. Distributions of electrons on v_z, v_θ, and v_r, shown in Fig. 3, shows that an increase in l leads to a decrease of $\langle v_z \rangle$ with a corresponding increase of $\langle v_\theta \rangle$. While $\langle v_r \rangle = 0$ the spread of the momentum increases only slightly as a function of l.

The values for $\langle v_z \rangle$, $\langle v_\theta \rangle$, and $\langle rv_\theta \rangle$ are given in Table II, in agreement with Eq. (13), a linear relationship is found between the axial and orbital momenta. In the nonrelativistic regime it becomes $krv_\theta/c = lv_z/c + A$ a linear fit to $l\langle v_z \rangle/c$ versus $k\langle rv_\theta \rangle/c$ is fulfilled with a proportionality coefficient of 0.94 $\pm$0.02, and a constant value of $A = -0.02$ $\pm$0.02. This relation is shown graphically in Fig. 4. A difference of the proportionality coefficient from the expected value of 1 is due to a small average radial displacement of electrons

TABLE II. Average velocity and orbital momentum components as a function of azimuthal mode number l, the averages in the second, third, and fourth columns are plotted in Fig. 3, the averages and errors are calculated from Gaussian function fits, with an error of 2×10^{-2} for $\langle v_z \rangle$ and 10^{-3} for the remaining averages. There is a linear relationship between $l\langle v_z \rangle$ and $k\langle rv_\theta \rangle$ with a gradient of 0.94 $\pm$0.02.

Mode no. l	$\langle v_z \rangle$ (c)	$\langle v_\theta \rangle$ (c)	$\langle rv_\theta \rangle$ ($c^2\omega_{\rm pe}^{-1}$)
0	0.70	0.00	0.00
1	0.67	0.07	0.32
2	0.66	0.12	0.64
4	0.63	0.17	1.25

and due to relativistic corrections which are not considered in Eq. (13). Thus, relation (13) explains a proportionality between the axial and angular momentum transfer observed in the linear regime in Ref. [11].

D. Angular momentum transfer

The distribution of the density of angular momentum, $n_e l_z$, as a function of electron axial momentum, p_z, can be seen as in Fig. 4(a). It is convenient to overlay the negative and positive

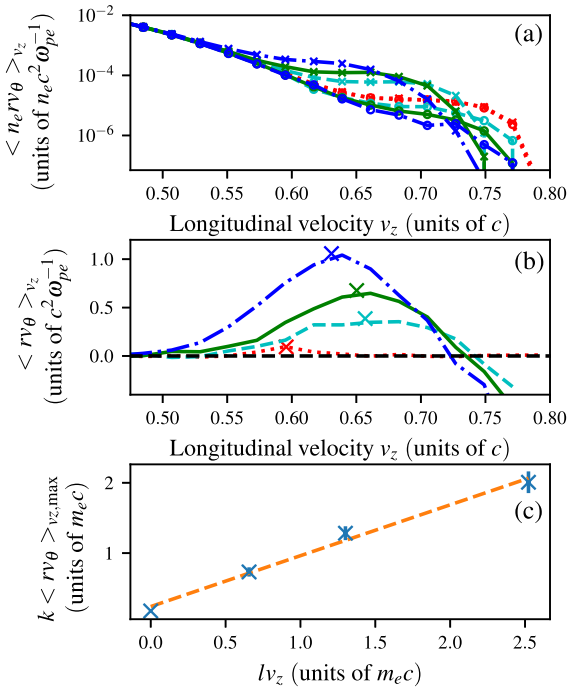

FIG. 4. Dependence of the orbital momentum density $n_e l_z/\gamma m_e$ at a time $t = 6.3\ T_{\rm pe}$. Plot (a) shows the distribution of the positive and negative parts of $n_e l_z$ ($\times$ for positive, $\circ$ for negative). Plot (b) shows $\langle l_z \rangle$ as a function of p_z. The $\times$ markers show the peak $\langle l_z \rangle$ used in the bottom plot; this peak is found by fitting the curve by a Gaussian function panels a) and b) use the same line styles as displayed in the legend in 2. Plot (c) shows the peak in $k\langle l_z \rangle_{p_z}$ as a function of lp_z with a linear best fit, the gradient of this fit is 0.9 ± 0.2, the intercept $A = 0.04$ $\pm$0.05. The lines shown here are smoothed using a moving average over five bins.

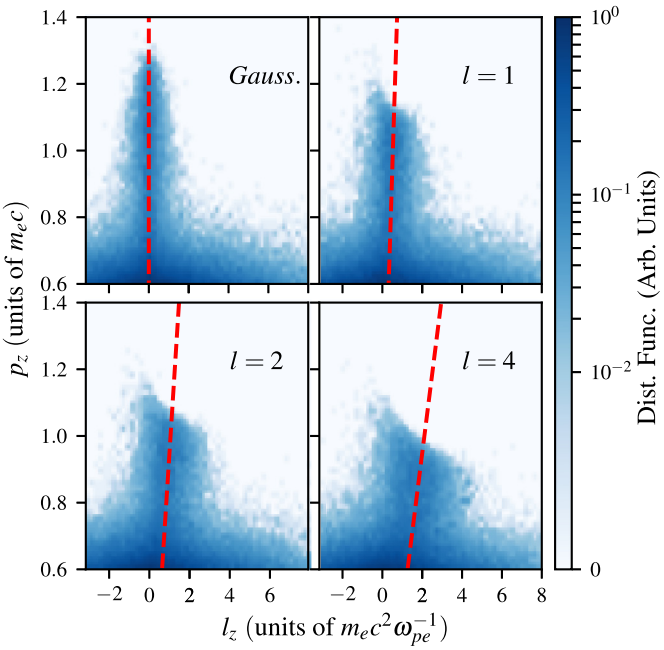

FIG. 5. Plots showing the distribution of l_z and p_z among accelerated particles taken at a time $t = 6.3\ T_{\rm pe}$. The red dashed lines show plots of Eq. (13) for $A = 0$.

$n_e l_z$ so that the relative amount of $n_e l_z$ can be readily observed. For values of p_z in the range 0.7–1.1 $m_e c$ a net positive orbital angular momentum can be seen, while above a certain threshold ($\sim$1.05 $m_e c$ for $l = 4$, $\sim$1.1 $m_e c$ for $l = 2$, and $\sim$1.15 $m_e c$ for $l = 1$) orbital angular momentum is negative.

It can be seen in Fig. 4(b) that there is positive angular momentum associated with particles with a velocity close to $p_{\rm ph}$, where $p_{\rm ph} \sim 0.75$ is the approximate momentum an electron has while traveling at the phase velocity $v_{\rm ph} \sim 0.6$.

The linear relationship between the quantities $k\langle l_z\rangle|_{p_z}$ and $l p_z$ is shown in Fig. 4(c). Similar to the analysis of the average velocities, a linear relationship between the averaged $k\langle l_z\rangle$ as a function of $l p_z$ appears to be a good fit for the data with a proportionality of 0.9 $\pm$0.2. The distribution of l_z versus p_z is plotted as a 2D histogram in Fig. 5. This image also shows plots of Eq. (13) with a constant value of $A = 0$ to estimate spread of l_z away from this relationship. A greater spread in l_z can be seen for higher values of the azimuthal mode number l, with some particles still having significant logitudinal momentum without the associated OAM.

V. CONCLUSIONS

The presented study demonstrates, with use of 3D numerical simulations, the effect of nonlinear Landau damping of plasma waves carrying a nonzero orbital angular momentum. Several conclusive observations can be made from this study. The first, and most significant, is that particles are observed to be trapped in OAM plasma waves. These trapped electrons follow in a phase space with the same twisted geometry as the OAM plasma waves themselves. Figure 1 shows the same rotation in phase space for OAM plasma waves as is seen with planar waves when the space is transformed to take into account the phase rotation. In addition to this we find a direct relationship between the linear momentum transferred and the angular momentum in Eq. (13) that is supported by the PIC results shown in Fig. 4.

The second conclusion is that the energy distributions of electrons in damping Laguerre-Gaussian plasma waves are significantly changed as a function of azimuthal mode number. This dependence leads to larger numbers of lower energy particles, tending towards a significantly narrowed spread in gained energies for accelerated particles; see Fig. 2.

The third is that angular momentum is transferred from the plasma wave to the resonant electrons when Laguerre-Gaussian plasma waves are subject to Landau damping. The transfer of OAM and longitudinal momentum are proportional to each other; see Fig. 3 and Eq. (13).

Last, it is observed, from results shown in Fig. 4, that the damping of a plasma wave with a higher azimuthal mode number leads to a larger net orbital angular momentum l_z in particles traveling close to $v_{\rm ph}$; see Fig. 5 for the distribution of the OAM. This implies the existence of a population of electrons, with a longitudinal velocity close to the phase velocity of the plasma wave, that are orbiting the same center of rotation as the plasma wave.

ACKNOWLEDGMENTS

This work was granted access to HPC resources of TGCC under the allocation A0010506129 made by GENCI. We acknowledge PRACE for awarding us access to resource Joliot Curie-SKL based in France at the TGCC Center. The authors acknowledge support from the MEPhI Academic Excellence Project (Contract No. 02.a03.21.0005-27.08.2013). This research was partially supported by the Project LQ1606 with the financial support of the Ministry of Education, Youth and Sports as part of targeted support from the Czech National Programme of Sustainability II. This research was supported in part by The National Science Foundation (PHY 1903098).

APPENDIX: LANDAU DAMPING IN A 3D PIC ENVIRONMENT

There are several challenges in attempting to simulate linear Landau damping in a 3D PIC code in addition to the limit imposed by the bounce frequency ($E_0 \ll \gamma_L^2 m_e/ek$). One reason for this difficulty is that the linear theory is developed assuming a static distribution function—meaning that the Landau damping rate is strongly dependent on the gradient of the distribution function around the phase velocity of the wave in question ($df/dv_z|_{v_{\rm ph}\pm\delta v}$). Only particles with velocities similar to but less than the phase velocity contribute to the damping, conversely particles with velocities similar to but greater than the phase velocity give energy back to the wave. In a box without a steady supply of thermal electrons near the phase velocity the gradient in this region tends to 0 ($df/dv_z|_{v_{\rm ph}\pm\delta v} \to 0$), and at this point damping stops as there are equal numbers of particles either side of $v_{\rm ph}$.

The challenge is to find a regime where damping is strong enough to be observable while weak enough that some damping occurs before saturation, or even weak enough that the plasma can support a plasma wave at all. While it is possible

to use boundary conditions that will replace exiting electrons with a thermalized electrons, this creates problems in exciting a stable long-lived plasma wave. It is more convenient to use periodic boundary conditions in the direction of travel to maintain the progression of the wave through space. Using a longer box can help with this problem to some extent, though this is computationally very expensive, and so in this study a box $4\lambda_{\rm pe}$ long in the propagation direction is used.

For a driven plasma wave, the force equation, continuity, and Poisson equations are

$$m_e \partial_t \mathbf{u}_{\rm pe} - e\nabla\phi_{\rm pe} = -e\mathbf{E}_d, \tag{A1}$$

$$\partial_t \delta n_e + n_0 \nabla \cdot \mathbf{u}_{\rm pe} = 0, \tag{A2}$$

$$\nabla^2 \phi_{\rm pe} = \delta n_e \frac{e}{\varepsilon_0}, \tag{A3}$$

where $\mathbf{u}_{\rm pe}, \phi_{\rm pe}, \delta n_e$ are the perturbation velocity, potential, and charge density, respectively, while $\mathbf{E}_d$ is an imposed driving electric field of the form required; see Eqs. (10), (11), and (12) for the form used in this study. The following forced oscillation equation for the plasma wave electric field can be found from this:

$$\partial_t^2 \mathbf{E}_{\rm pe} + \omega_{\rm pe}^2 \mathbf{E}_{\rm pe} = \omega_{\rm pe}^2 \mathbf{E}_d, \tag{A4}$$

where $\mathbf{E}_{\rm pe}$ is the electric field associated with the plasma wave. If we put in an oscillating field of the form $\mathbf{E}_d = \hat{\mathbf{e}}_s E_0 \cos(\omega_{\rm pe} t)$, where $\hat{\mathbf{e}}_s$ is the unit vector associated with the s component and E_0 is the amplitude of the imposed field, the solution gives an $\mathbf{E}_{\rm pe}$ out of phase with $\mathbf{E}_d$. The solution for $\mathbf{E}_{\rm pe}$ in this case is

$$\mathbf{E}_{\rm pe} = \hat{\mathbf{e}}_s \frac{\omega_{\rm pe} E_0 t \sin(\omega_{\rm pe} t)}{2}, \tag{A5}$$

where E_0 is the amplitude of the wave and t is the time over which the driving electric field is imposed. While the growth of the electric field in this case is linear, there are second-order effects, such as small magnetic fields, which may be amplified much quicker. However, if the driving term small enough ($\mathbf{E}_d \ll \mathbf{E}_{\rm pe}$), we can get close to a situation where the second-order effects are suppressed. This method avoids amplifying the plasma wave too quickly into regimes where wave breaking or other large amplitude coupling occurs, it is also similar to the method presented in Ref. [19]. Frequency matching is important for good coupling, the frequency of the driving force is chosen using Eq. (6). The rate of Landau damping in the linear regime is independent of the amplitude of the wave and so acts to reduce the maximum achievable plasma wave amplitude. Once the wave enters the transition stage to nonlinear behavior (when $\omega_b > \gamma_L$) the frequency of the wave also changes and the frequency of the driving electric field becomes slightly mismatched.

[1] L. Allen, M. W. Beijersbergen, R. J. C. Spreeuw, and J. P. Woerdman, Orbital angular momentum of light and the transformation of Laguerre-Gaussian laser modes, Phys. Rev. A **45**, 8185 (1992).

[2] Q. Zhan, Cylindrical vector beams: From mathematical concepts to applications, Adv. Opt. Photonics **1**, 1 (2009).

[3] J. Vieira and J. T. Mendonça, Nonlinear Laser Driven Donut Wakefields for Positron and Electron Acceleration, Phys. Rev. Lett. **112**, 215001 (2014).

[4] Z. Lécz, A. Andreev, and A. Seryi, Plasma rotation with circularly polarized laser pulse, Laser Part. Beams **34**, 31 (2016).

[5] J. Vieira, J. T. Mendonça, and F. Quéré, Optical Control of the Topology of Laser-Plasma Accelerators, Phys. Rev. Lett. **121**, 054801 (2018).

[6] R. Nuter, P. Korneev, I. Thiele, and V. T. Tikhonchuk, Plasma solenoid driven by a laser beam carrying an orbital angular momentum, Phys. Rev. E **98**, 033211 (2018).

[7] J. T. Mendonça, S. Ali, and B. Thidé, Plasmons with orbital angular momentum, Phys. Plasmas **16**, 112103 (2009).

[8] D. R. Blackman, R. Nuter, P. Korneev, and V. T. Tikhonchuk, Kinetic plasma waves carrying orbital angular momentum, Phys. Rev. E **100**, 013204 (2019).

[9] Y. Shi, J. Vieira, R. M. G. M. Trines, R. Bingham, B. F. Shen, and R. J. Kingham, Magnetic Field Generation in Plasma Waves Driven by Copropagating Intense Twisted Lasers, Phys. Rev. Lett. **121**, 145002 (2018).

[10] J. T. Mendonça, Kinetic description of electron plasma waves with orbital angular momentum, Phys. Plasmas **19**, 112113 (2012).

[11] D. R. Blackman, R. Nuter, P. Korneev, and V. T. Tikhonchuk, Twisted kinetic plasma waves, J. Russ. Laser Res. **40**, 419 (2019).

[12] R. Nuter and V. Tikhonchuk, Prepulse suppression and optimization of backward Raman amplification with a chirped pump laser beam, Phys. Rev. E **87**, 043109 (2013).

[13] G. E. P. Box and M. E. A Muller, Note on the generation of random normal deviates, Ann. Math. Statist. **29**, 610 (1958).

[14] L. Devroye, *Non-Uniform Random Variate Generation* (Springer, New York, 1986).

[15] W. Kruer, *The Physics of Laser Plasma Interactions* (Addison-Wesley–CRC Press, Redwood, CA, 1988).

[16] W. M. Manheimer and R. W. Flynn, Formation of stationary large amplitude waves in plasmas, Phys. Fluids **14**, 2393 (1971).

[17] G. J. Morales and T. M. O'Neil, Nonlinear Frequency Shift of an Electron Plasma Wave, Phys. Rev. Lett. **28**, 417 (1972).

[18] R. L. Dewar, Frequency shift due to trapped particles, Phys. Fluids **15**, 712 (1972).

[19] N. A. Yampolsky and N. J. Fisch, Simplified model of nonlinear Landau damping, Phys. Plasmas **16**, 072104 (2009).